Electronic Supplementary Information

Unravelling the need for balancing band convergence and resonant level in $Sn_{1-x-y}In_xMn_yTe$ for high thermoelectric performance

Shantanu Misra[1], Bartlomiej Wiendlocha[2,*], Soufiane El Oualid[1], Anne Dauscher[1], Bertrand Lenoir[1], Christophe Candolfi[1,*]

[1] *Institut Jean Lamour, UMR 7198 CNRS – Université de Lorraine, Campus ARTEM, 2 allée André Guinier, BP 50840, 54011 Nancy, France*

[2] *AGH University of Krakow, Faculty of Physics and Applied Computer Science, Aleja Mickiewicza 30, 30-059 Krakow, Poland*

[*]Contact authors: wiendlocha@fis.agh.edu.pl ; christophe.candolfi@univ-lorraine.fr

Content

Figure S4. Additional secondary electron (SE) and backscattered electron (BSE) images and their corresponding elemental mapping of the (x,y) = (0.02, 0.02) and (x,y) = (0.02, 0.08) samples.

Figure S5. Bloch spectral functions, calculated for $Sn_{0.9375}Mn_{0.06}In_{0.025}Te$, in ferromagnetic state.

Figure S6. Low-temperature dependence of the a) hole concentration p and b) Hall mobility μ_H for the series $Sn_{0.94-x}In_xMn_{0.06}Te$ for $0.0 \leq x \leq 0.025$.

Figure S7. Residual electrical resistivity ρ_0 and Hall mobility μ_0 measured at 5 K as a function of the concentration of various doping elements and for the series $Sn_{0.94-x}In_xMn_{0.06}Te$ ($0.0 \leq x \leq 0.025$).

Equations of the Klemens-Callaway model.

Figure S8. Temperature dependence of the Lorenz number L of the $Sn_{0.94}Mn_{0.06}Te$ sample determined from the SPB model and deduced from the experimental κ_L data.

Figure S9. Temperature dependence of the thermoelectric properties of the series $Sn_{0.99-y}In_{0.01}Mn_yTe$ for y = 0.05, 0.06 and 0.07.

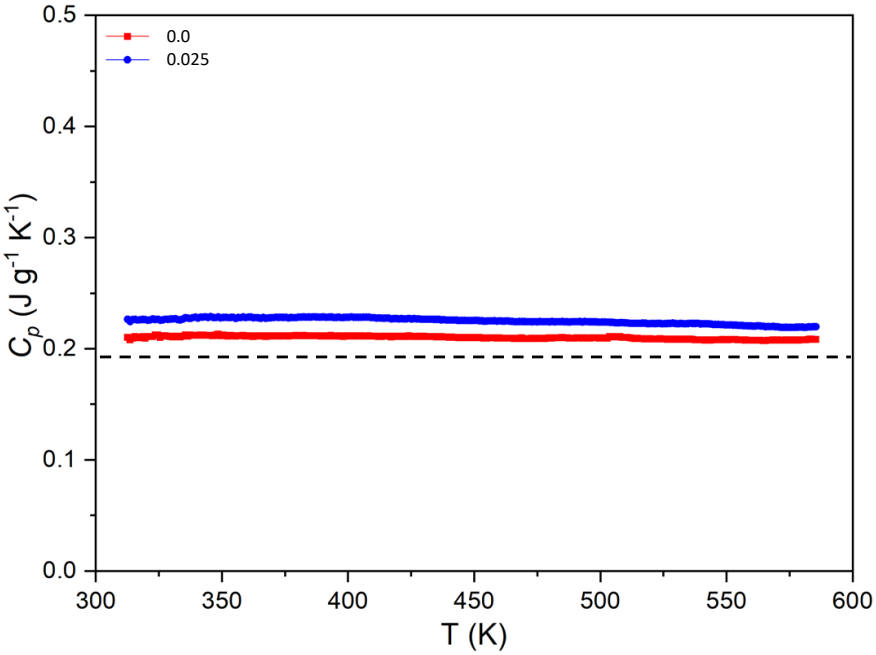

Figure S1. Temperature dependence of the isobaric specific heat C_p of the $Sn_{0.94-x}In_xMn_{0.06}Te$ samples for x = 0.0 and 0.025 used to calculate the total thermal conductivity of the samples above 300 K. The data were fitted and extrapolated up to 850 K. For both samples, the measured C_p values are higher than the Dulong-Petit limit equal to 0.1973 (horizontal dashed line) and 0.2057 J g^{-1} K^{-1} for the binary SnTe and $Sn_{0.94}Mn_{0.06}Te$, respectively.

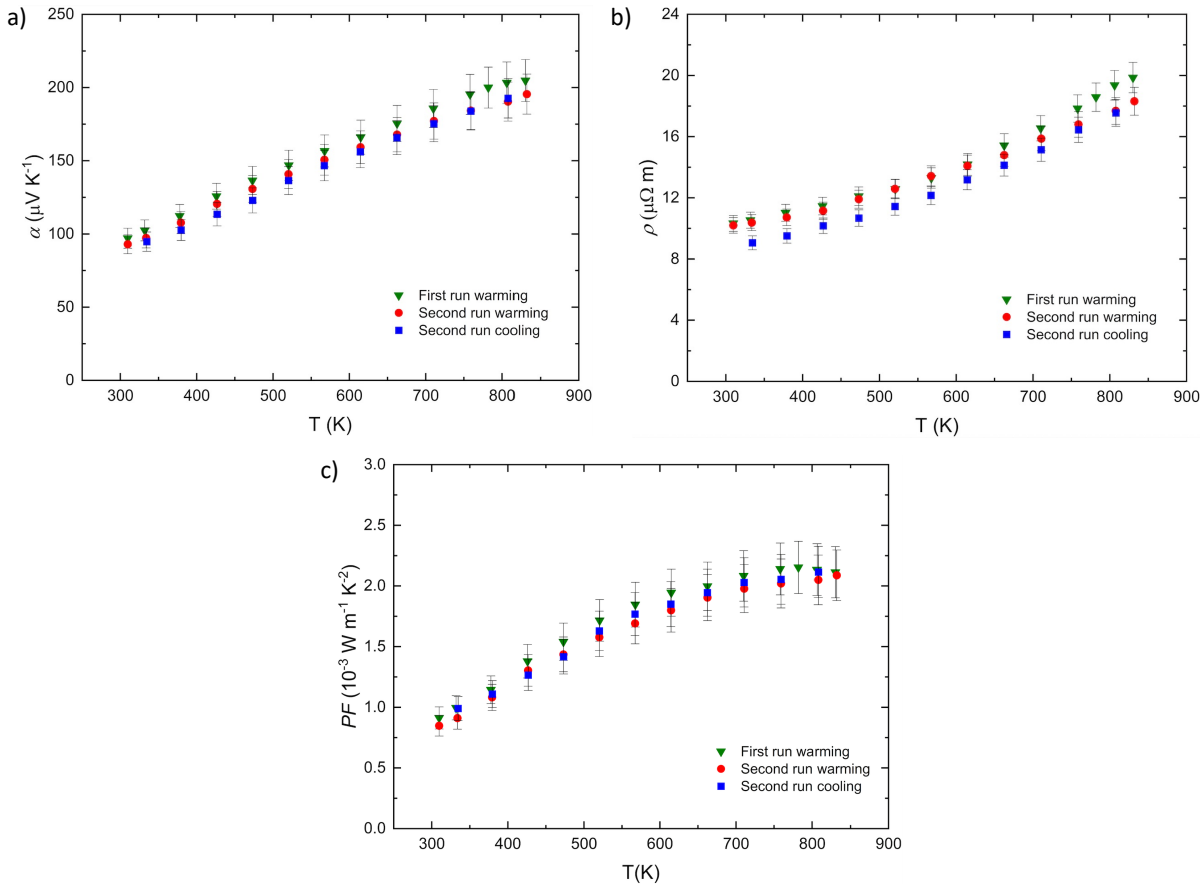

Figure S2. Second measurement of the temperature dependence of the a) thermopower α, b) electrical resistivity ρ and power factor PF of the (x,y) = (0.01, 0.06) sample performed upon warming and cooling. The data are compared to those obtained during the first measurement shown in the main text for which only data upon warming have been collected. The error bars correspond to the experimental uncertainty mentioned in the main text.

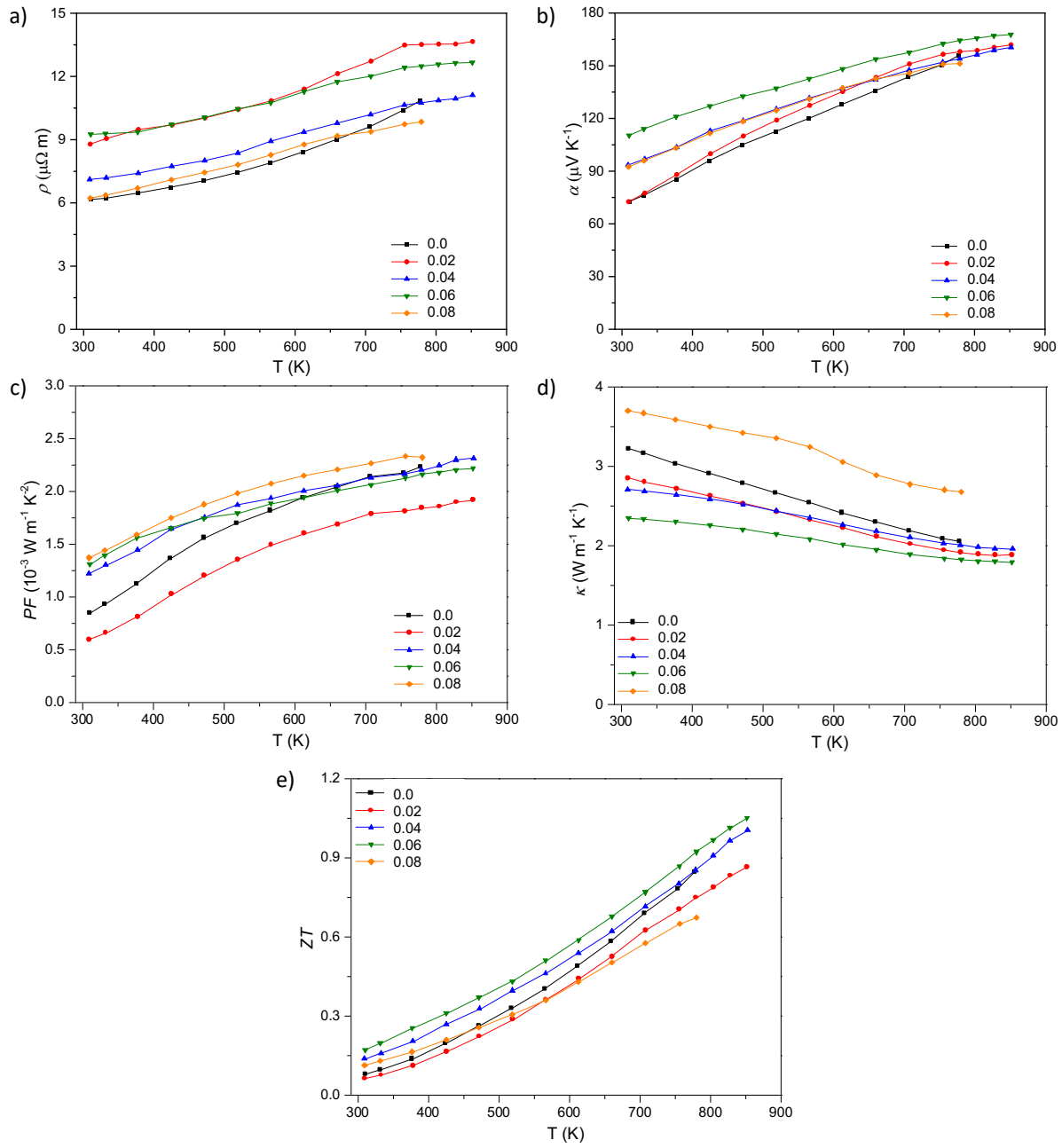

Figure S3. Temperature dependence of the a) electrical resistivity ρ, b) thermopower α, c) power factor *PF*, d) total thermal conductivity and e) dimensionless thermoelectric figure of merit *ZT* for the series $Sn_{0.98-y}In_{0.02}Mn_yTe$ for $0.0 \leq y \leq 0.08$. In all panels, the solid lines are a guide to the eye. The optimum thermoelectric properties are obtained for the (x, y) = (0.02, 0.06) sample, which served as a starting point for our study.

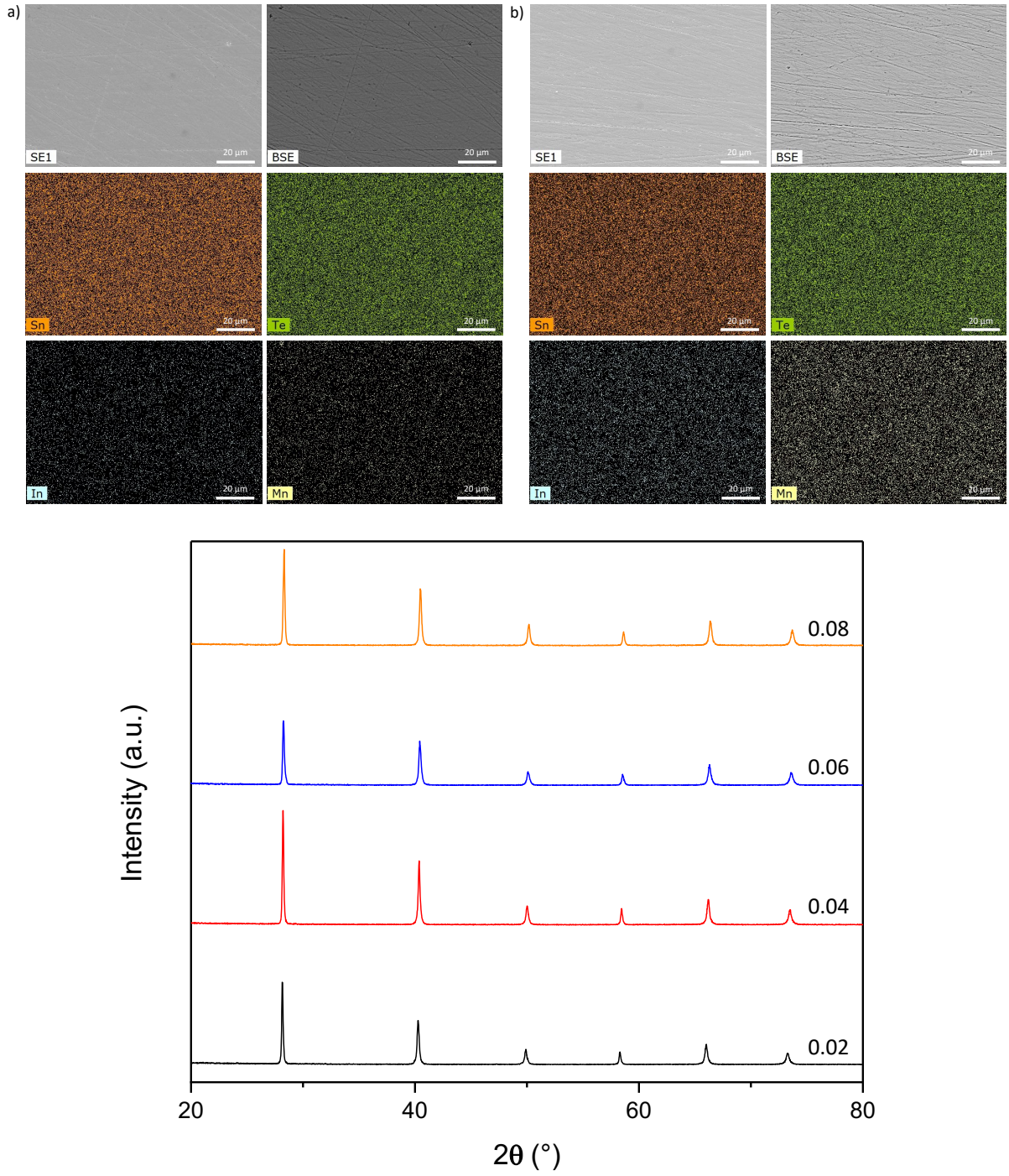

Figure S4. (upper panels) Secondary electron (SE) and backscattered electron (BSE) images and their corresponding elemental mapping of the a) (x,y) = (0.02, 0.02) and b) (x,y) = (0.02, 0.08) samples, showing the homogeneous distribution of all the elements. No Mn-rich phases are thus observed up to 8% in this series. (lower panel) PXRD patterns of the (x = 0.02, y) series for y = 0.02, 0.04, 0.06 and 0.08.

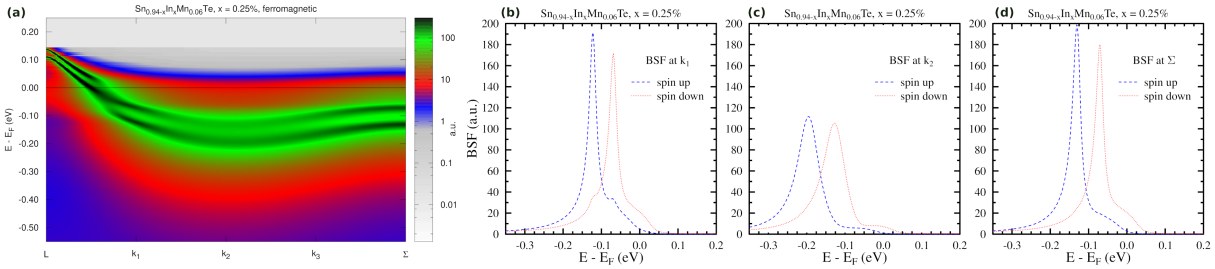

Figure S5. Bloch spectral functions, calculated for $Sn_{0.9375}Mn_{0.06}In_{0.025}Te$, in ferromagnetic state. The figure has the same format as Figure 4 in the main text. Both spin up and spin down BSFs are plotted in panel (a) and the band splitting due to ferromagnetism induced by Mn is visible. In panels (b-d), BSFs are plotted at k-points k_1, k_2 and Σ, indicated in the plot in panel (a). Comparing the results to those in Figure 4, we can observe that the magnetic disorder, simulated using the disordered local moments state in Figure 4, does not induce any additional visible band smearing in addition to that related to the already-present resonant effect.

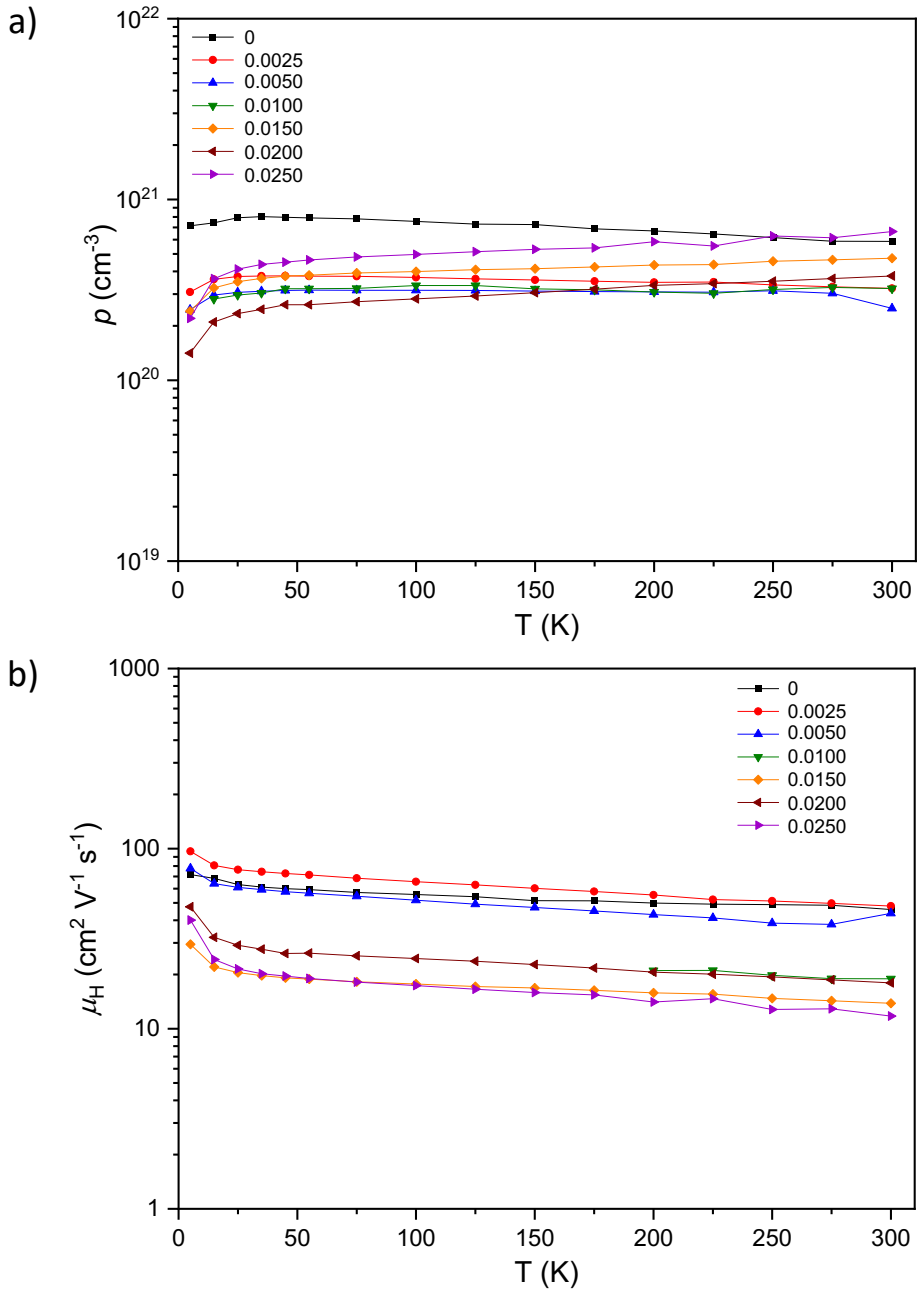

Figure S6. Temperature dependence of the a) hole concentration p and b) Hall mobility μ_H for the series $Sn_{0.94-x}In_xMn_{0.06}Te$ for $0.0 \leq x \leq 0.025$. The slight downturn and upturn in p and μ_H, respectively, observed at low temperatures are due to a magnetic transition, reported in prior studies on $Sn_{1-y}Mn_yTe$, which is still present in the In-containing samples. In both panels, the solid lines are a guide to the eye.

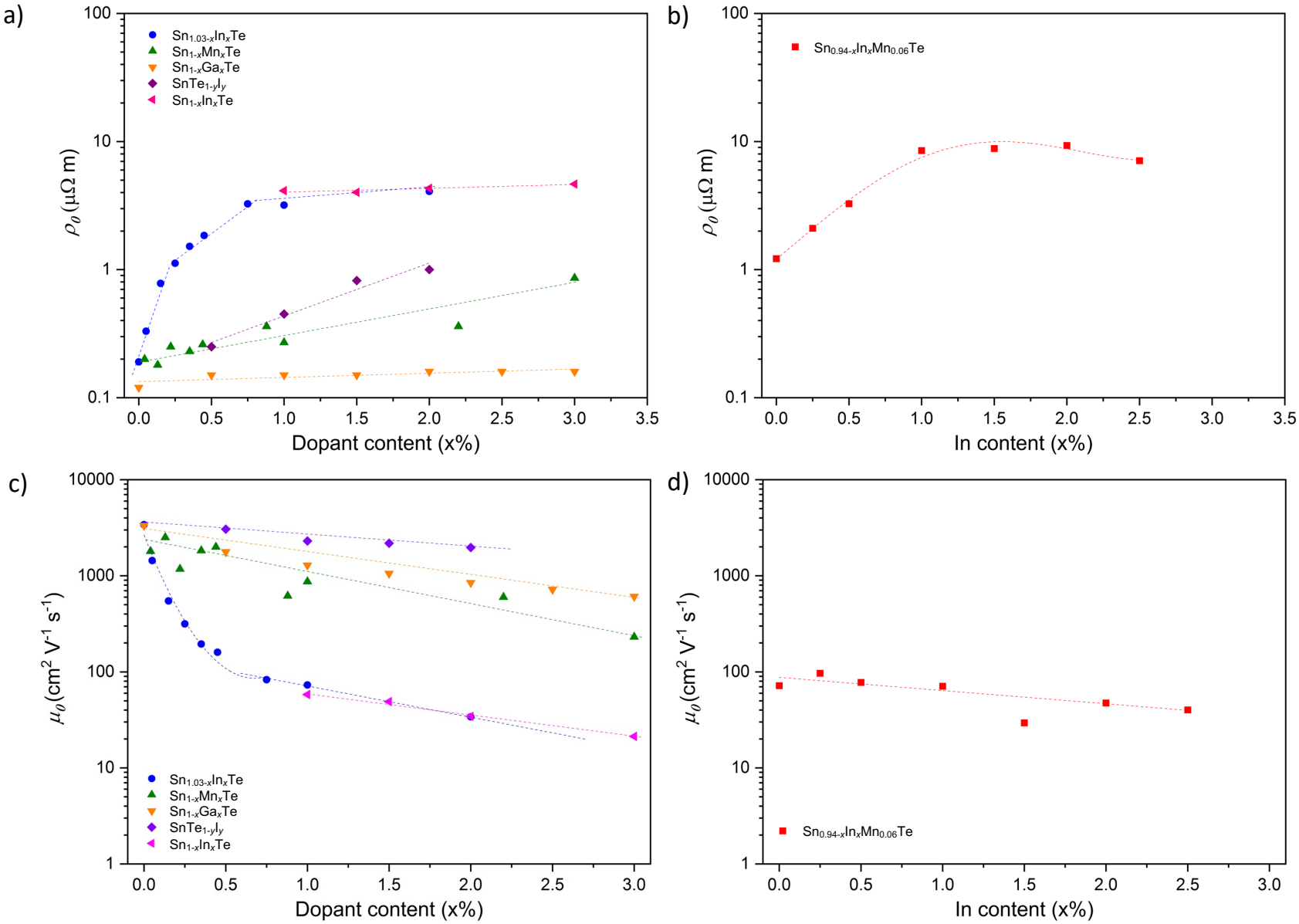
a)
b)
c)
d)
$Sn_{1.03-x}In_xTe$
$Sn_{1-x}Mn_xTe$
$Sn_{1-x}Ga_xTe$
$SnTe_{1-y}I_y$
$Sn_{1-x}In_xTe$
$Sn_{0.94-x}In_xMn_{0.06}Te$
ρ_0 (μΩ m)
μ_0 (cm^2 V^{-1} s^{-1})
Dopant content (x%)
In content (x%)

Figure S7. Residual electrical resistivity ρ_0 (panels a and b) and Hall mobility μ_0 (panels c and d) measured at 5 K as a function of the concentration of various doping elements and for the series $Sn_{0.94-x}In_xMn_{0.06}Te$ ($0.0 \leq x \leq 0.025$). For comparison purposes, the data obtained on the series $Sn_{1.03-x}In_xTe$ and $Sn_{1-x}In_xTe$ have been added. Data for the series $Sn_{1-x}Mn_xTe$ have been taken from the literature (Ref. S1, S2 and S3; data measured at 5 K) and completed by calculations and calculated for the series $Sn_{1-x}Ga_xTe$ and $SnTe_{1-y}I_y$ (no measurements at 5 K available in the literature).

Klemens-Callaway modeling

The rather high level of alloying in the series $Sn_{1-x-y}In_xMn_yTe$ enhances point-defect scattering of phonons due to mass fluctuations and strain field effects, which both contribute to lower κ_L. The magnitude of the alloying effect of In and Mn on κ_L was quantified using the Klemens-Callaway model. The lattice thermal conductivity of the alloyed compounds $\kappa_{L,A}$ was calculated using the thermal conductivity of the pure end-member compounds, $\kappa_{L,P}$, and assuming that both Umklapp and point-defect scattering processes dominate[S4,S5]

$$\frac{\kappa_{L,A}}{\kappa_{L,P}} = \frac{\arctan(u)}{u}$$

$$u^2 = \frac{\pi\theta_D\Omega}{2h\,\upsilon^2}\,\kappa_{L,P}\Gamma$$

In these relations, Ω is the average volume per atom, θ_D is the Debye temperature, h is the Planck constant, υ is the average speed of sound measured on the pure compounds and Γ is the scattering parameter defined as[S4,S6-S8]

$$\Gamma = \Gamma_{mass} + \Gamma_{strain\ field} = x(1-x)\left[\left(\frac{\Delta M}{M_{avg}}\right)^2 + \varepsilon\left(\frac{\Delta\delta}{\delta_{avg}}\right)^2\right]C$$

where x is the relative concentration of the impurity atom, M_{avg} and δ_{avg} are the average molar mass and atomic radius, respectively, ΔM and $\Delta\delta$ are the molar mass and atomic radius differences, respectively, between those of the substituting and substituted atoms. For a

compound of chemical formula $A_mB_{n(1-x)}S_{nx}$ where *B* is substituted by the atoms *S*, the parameter *C* is defined as follows[S7,S8]

$$C = \frac{n}{m+n}\frac{M_{avg}}{M_{tot}}$$

Where M_{tot} is the total molar mass as described in Ref. 4. Γ_{mass} corresponds to the scattering related to atomic mass contrast while $\Gamma_{strain\ field}$ describes the scattering due to the network distortion. In this model, ε is a phenomenological fitting parameter that can be related to the Grüneisen parameter characterizing the anharmonicity of the lattice vibrations.[S5] Typical values of ε fall within the range 10 – 100 for various thermoelectric materials.[S5]

Taking the covalent radii of the atoms for the parameter δ, this model predicts that the effect of In is negligible due to its molar mass similar to Sn and the negligible decrease in the lattice parameter induced. Upon Mn alloying, this model predicts a decrease in κ from 3.2 W m^{-1} K^{-1} for (x, y) = (0.02, 0.0) to 2.4 W m^{-1} K^{-1} at 300 K in the (x, y) = (0.02, 0.06) sample, in very good agreement with the experimental results (see Figure S3). The stronger decrease in κ observed in the (x, y) = (0.02, 0.0) sample upon heating is thus mostly due to the more pronounced increase in ρ. These results indicate that the additional decrease in κ achieved in the (x, y) = (0.01, 0.06) and (0.015, 0.06) samples is also due to a further reduction in κ_e reflecting the higher ρ values measured in these samples.

References

S1 M. Inoue, H. Yagi, K. Lshii, T. Tatsukawa, *J. Low Temp. Phys.*, 1976, **23**, 785.

S2 H. Chi, G. Tan, M. G. Kanatzidis, Q. Li, C. Uher, *Appl. Phys. Lett.*, 2016, **108**, 182101.

S3 M. Inoue, K. lshii, H. Yagi and T. Tatsukawa, Memoirs of the Faculty of Engineering, Fukui University, 1976, vol. 24, p. 237.

S4 J. Callaway, H. C. von Baeyer, *Phys. Rev.*, 1960, **120**, 1149−1154.

S5 P. G. Klemens, *Phys. Rev.*, 1960, **119**, 507−509.

S6 B. Abeles, *Phys. Rev.*, 1963, **131**, 1906−1911.

S7 G. A. Slack, *Phys. Rev.*, 1962, **126**, 427−441.

S8 G. P. Meisner, D. T. Morelli, S. Hu, J. Yang, C. Uher, *Phys. Rev. Lett.*, 1998, **80**, 3551−3554.

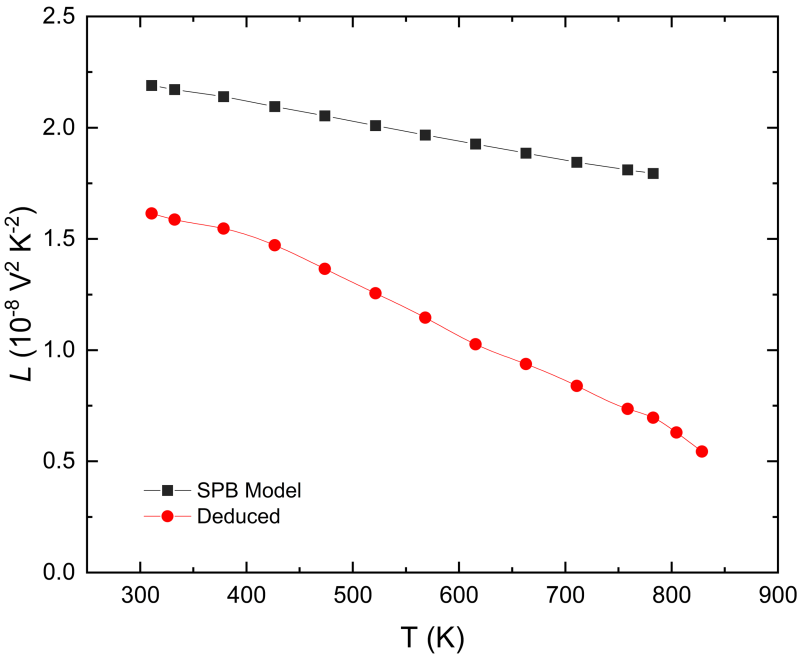

Figure S8. Temperature dependence of the Lorenz number L of the $Sn_{0.94}Mn_{0.06}Te$ sample determined from the SPB model and deduced from the experimental κ_L values of the (x, y) = (0.01, 0.06) sample by assuming that the κ_L values of $Sn_{0.94}Mn_{0.06}Te$ are similar. The solid lines are a guide to the eye.

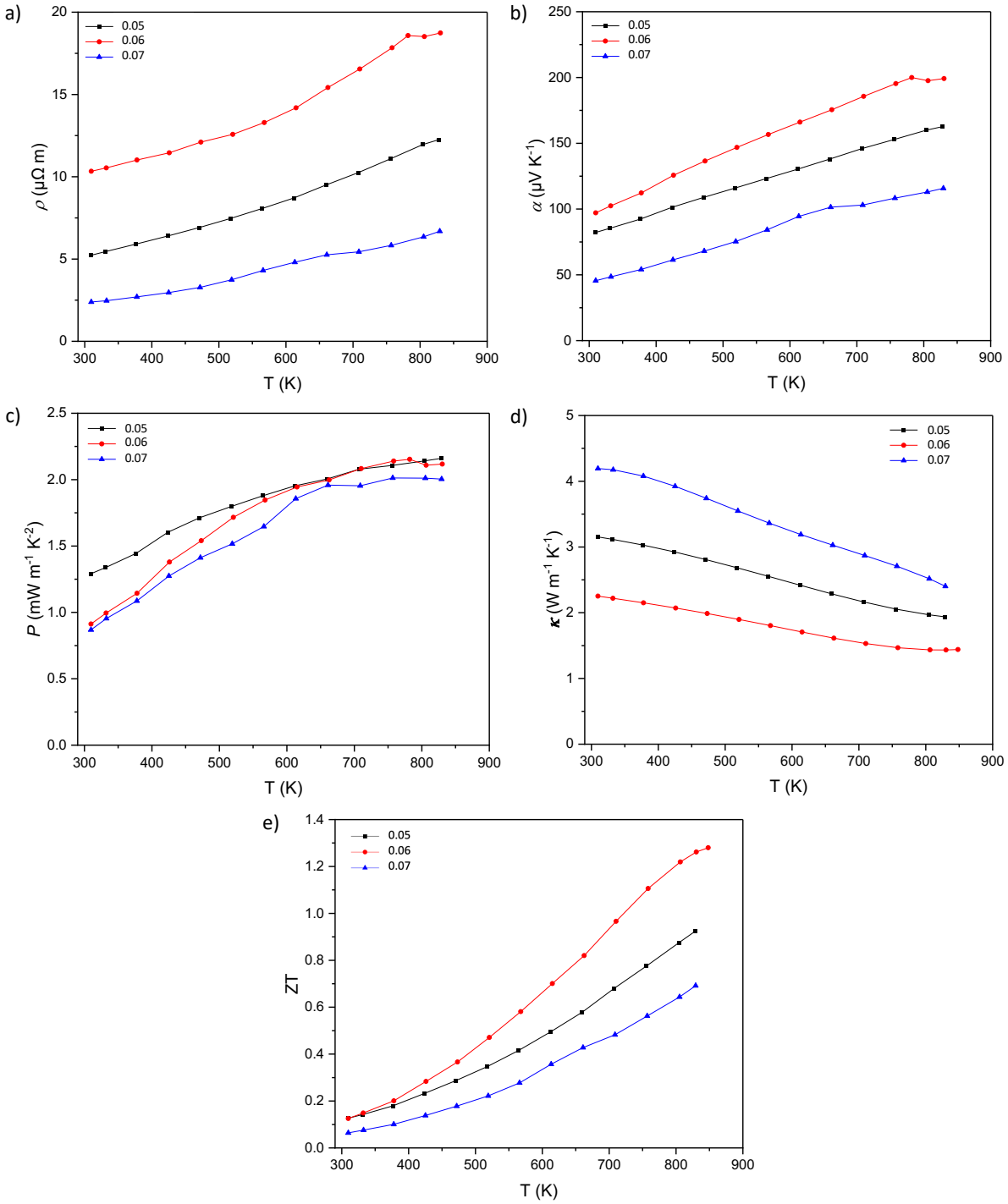

Figure S9. Temperature dependence of the a) electrical resistivity ρ, b) thermopower α, c) power factor P, d) total thermal conductivity κ and e) dimensionless thermoelectric figure of merit ZT of the series $Sn_{0.99-y}In_{0.01}Mn_yTe$ for y = 0.05, 0.06 and 0.07. In all panels, the solid lines are a guide to the eye.